International Conference on Mathematics, Computational Methods & Reactor Physics (M&C 2009)
Saratoga Springs, New York, May 3-7, 2009, on CD-ROM, American Nuclear Society, LaGrange Park, IL (2009)

HIGH-ORDER DISCRETE ORDINATE TRANSPORT IN NON-CONFORMING 2D CARTESIAN MESHES

L. Gastaldo, R. Le Tellier, C. Suteau,
D. Fournier and J.M. Ruggieri
CEA Cadarache
DEN/DER/SPRC/LEPh
Building 230, 13108 Saint Paul-lez-Durance, France
laura.gastaldo@cea.fr; romain.le-tellier@cea.fr; christophe.suteau@cea.fr;
damien.fournier@cea.fr; jean-michel.ruggieri@cea.fr

ABSTRACT

We present in this paper a numerical scheme for solving the time-independent first-order form of the Boltzmann equation in non-conforming 2D Cartesian meshes. The flux solution technique used here is the discrete ordinate method and the spatial discretization is based on discontinuous finite elements. In order to have p-refinement capability, we have chosen a hierarchical polynomial basis based on Legendre polynomials. The h-refinement capability is also available and the element interface treatment has been simplified by the use of special functions decomposed over the mesh entities of an element. The comparison to a classical S_N method using the Diamond Differencing scheme as spatial approximation confirms the good behaviour of the method.

Key Words: Discrete Ordinate Method, Discontinuous Finite Element Method, Non-Conforming Mesh

1. INTRODUCTION

The time-independent first-order form of the Boltzmann equation can be used to represent the behaviour of a stationnary population of neutral particles. In this paper we will only consider the one-speed form of the Boltzmann equation and we use the discrete ordinate approximation with a standard level-symmetric quadrature (LS_N) to discretize the angular variable.
The discrete ordinate equation for a single energy group and a given direction $\vec{\Omega}_n$ can be written as [1] :

$$\vec{\Omega}_n \cdot \vec{\nabla}\phi_n(\vec{r}) + \Sigma_t(\vec{r})\phi_n(\vec{r}) = q_n(\vec{r}) \tag{1}$$

where $\phi_n(\vec{r}) = \phi(\vec{r}, \vec{\Omega}_n)$ represents the neutron flux in the fixed direction $\vec{\Omega}_n$, $\Sigma_t(\vec{r})$ is the macroscopic total cross section and $q_n(\vec{r}) = q(\vec{r}, \vec{\Omega}_n)$ is the neutron source in the fixed direction, containing external sources as well as those resulting from the scattering from other directions. Functions $\phi_n(\vec{r})$, $\Sigma_t(\vec{r})$ and $q_n(\vec{r})$ are defined over a domain $\mathcal{D}$ which is assumed to be open, bounded, convex region in $\mathbb{R}^2$.
As boundary conditions, we specify the flux entering $\mathcal{D}$ from outside through the surface $\Gamma = \partial\mathcal{D}$:

$$\phi_n(\vec{r}) = \phi_n^{BC}(\vec{r}), \qquad \text{for} \quad \vec{r} \in \Gamma^-$$

where the inflow Γ^- is given by :

$$\Gamma^- = \{\vec{r} \in \Gamma \, : \, \vec{\Omega}_n \cdot \vec{n}(\vec{r}) < 0\}$$

and $\vec{n}(\vec{r})$ is the unit outward normal vector to Γ at $\vec{r} \in \Gamma$.

In [2], a transport solver has been developed based on a discontinuous finite element formulation with linear and quadratic shape functions. This solver has mesh adaptation capabilities. The purpose of this paper is to present a method for solving S_N equations on two-dimensional non-conforming Cartesian meshes easily extensible to 3D non-conforming hexahedral grids and allowing us to have not only h-refinement capability but also p-refinement capability. Concerning the mesh refinement, following [3], we choose a cell-by-cell mesh refinement since it better deals with local physics. But, unlike [3] we don't have to refine the cells in equal parts. Such advanced capabilities are of particular interest for treating computationally demanding benchmarks (e.g. [4]).

This paper is organized as follows. In the next section we describe the discontinuous finite element method applied to the spatial differencing of the S_N equations on 2D Cartesian meshes. This method uses a hierarchical polynomial basis based on Legendre polynomials, which is presented in the third section. Then, in order to deal with non-conforming meshes, a cell interface transformation is presented. In the last section, we give some numerical results which confirm the good behaviour of the method.

2. DISCONTINUOUS FINITE ELEMENT DISCRETIZATION

Let $\mathcal{M}_h$ be a regular decomposition of the domain $\mathcal{D}$ into quadrilateral elements κ. By $\mathcal{E}_h$ (respectively $\mathcal{E}_h(\kappa)$) we denote the set of all edges e of the mesh (respectively of the element $\kappa \in \mathcal{M}_h$). The set of edges included in the boundary of $\mathcal{D}$ is denoted by $\mathcal{E}_h^\partial$ and the set of internal ones (*i.e.* $\mathcal{E}_h \setminus \mathcal{E}_h^\partial$) is denoted by $\mathcal{E}_h^\circ$. For each edge of the mesh $e \in \mathcal{E}_h(\kappa)$, $\vec{n}$ stands for the outward normal vector of e.
Let V_h^p be the space of discontinuous piecewise polynomials of degree $p \geq 0$:

$$V_h^p = \{v \in L^2(\mathcal{D}) \,:\, v|_\kappa \in Q_p(\kappa) \quad \kappa \in \mathcal{M}_h\}$$

where $Q_p(\kappa)$ is the space of polynomials of degree p or less on κ.
Multiplying equation (1) by a function $v_h \in V_h^p$, integrating by parts over each cell $\kappa \in \mathcal{M}_h$ and taking the sum over $\mathcal{M}_h$, we get :

$$\begin{aligned}\sum_{\kappa\in\mathcal{M}_h} \int_\kappa (-\phi_{n,h}(\vec{\Omega}_n \cdot \vec{\nabla} v_h) + \Sigma_t\, \phi_{n,h}\, v_h)\, dr + \int_{e\in\mathcal{E}_h^\circ} F(\vec{\Omega}_n, \phi_{n,h}) \cdot [v_h]\, ds \\ = \int_\mathcal{D} q_n\, v_h\, dr - \int_{e\in\mathcal{E}_h^\partial\cap\Gamma^-} (\vec{\Omega}_n \cdot \vec{n})\, \phi_n^{BC}\, v_h\, ds, \qquad v_h \in V_h^p.\end{aligned} \tag{2}$$

where $F(\vec{\Omega}_n, \phi_{n,h})$ is the numerical flux function associated to this scheme and is defined as the upwind value of $\vec{\Omega}_n\phi_{n,h}$ given, for any interior edge shared by elements κ and κ', $e = \kappa|\kappa'$, by :

$$F(\vec{\Omega}_n, \phi_{n,h}) = \left| \begin{array}{ll} \vec{\Omega}_n \phi_{n,h}|_{e\cap\mathcal{E}_h(\kappa)} & \text{if } \vec{\Omega}_n \cdot \vec{n} > 0 \\ \vec{\Omega}_n \phi_{n,h}|_{e\cap\mathcal{E}_h(\kappa')} & \text{if } \vec{\Omega}_n \cdot \vec{n} < 0 \end{array} \right.$$

In the previous equation, $[v_h]$ is the jump of v_h across the edge $e = \kappa|\kappa'$ defined as :

$$[v_h] = v_h|_{e\cap\mathcal{E}_h(\kappa)}\, \vec{n} + v_h|_{e\cap\mathcal{E}_h(\kappa')}\, \vec{n'}, \qquad \forall v \in V_h^p$$

where $\vec{n'}$ is the unit normal on e pointing exterior to κ'.
For the sake of simplicity, for any $e \in \mathcal{E}_h^\circ$, $e = \kappa|\kappa'$, we will denote the interior trace of v on e by $v|_{e\cap\mathcal{E}_h(\kappa)} = v^+$ and the exterior trace of v on e by $v|_{e\cap\mathcal{E}_h(\kappa')} = v^-$, $\forall v \in V_h^p$. For a boundary edge, $e \in \mathcal{E}_h^\partial \cap \Gamma^-$, the exterior trace definition can be extended in the following manner :

$$v^- = v|_{\Gamma^-}, \qquad \forall v \in V_h^p$$

Moreover, let the inflow and outflow parts of $\mathcal{E}_h(\kappa)$ be written respectively as :

$$\begin{aligned}
\mathcal{E}_h^-(\kappa) &= \left\{ e \in \mathcal{E}_h(\kappa) : \vec{\Omega}_n \cdot \vec{n} < 0 \right\} \\
\mathcal{E}_h^+(\kappa) &= \left\{ e \in \mathcal{E}_h(\kappa) : \vec{\Omega}_n \cdot \vec{n} \geq 0 \right\}
\end{aligned}$$

Using these notations (2) can be rewritten as :

$$\begin{aligned}
\sum_{\kappa\in\mathcal{M}_h} \left[\int_\kappa (-\phi_{n,h}(\vec{\Omega}_n \cdot \vec{\nabla} v_h) + \Sigma_t \, \phi_{n,h} \, v_h) \, dr \right] & \\
+ \sum_{\kappa\in\mathcal{M}_h} \left[\sum_{e\in\mathcal{E}_h^\circ\cap\mathcal{E}_h^+(\kappa)} \int_e (\vec{\Omega}_n \cdot \vec{n}) \, \phi_{n,h}^+ \, v_h^+ \, ds + \sum_{e\in\mathcal{E}_h^\circ\cap\mathcal{E}_h^-(\kappa)} \int_e (\vec{\Omega}_n \cdot \vec{n}) \, \phi_{n,h}^- \, v_h^+ \, ds \right] & \\
= \int_\mathcal{D} q_n \, v_h \, dr - \int_{e\in\mathcal{E}_h^\partial\cap\Gamma^-} (\vec{\Omega}_n \cdot \vec{n}) \, \phi_n^{BC} \, v_h^+ \, ds, \qquad v_h \in V_h^p &
\end{aligned}$$

Integrating by parts over each cell $\kappa \in \mathcal{M}_h$ and considering that, as this stage, it is the interior trace $\phi_{n,h}^+$ that appears in the surface integral, we obtain the Discontinuous Galerkin approximation (see [5], and [6]) of the model problem (1), which can be compactly written as [7] :

$$\begin{aligned}
&\text{find} \quad \phi_{n,h} \in V_h^p \quad \text{such that} \quad \forall v_h \in V_h^p \\
&\sum_{\kappa\in\mathcal{M}_h} \left[\int_\kappa (v_h(\vec{\Omega}_n \cdot \vec{\nabla}\phi_{n,h}) + \Sigma_t \, \phi_{n,h} \, v_h) \, dr - \sum_{e\in\mathcal{E}_h\cap\mathcal{E}_h^-(\kappa)} \int_e (\vec{\Omega}_n \cdot \vec{n}) \, \phi_{n,h}^+ \, v_h^+ \, ds \right] \\
&\qquad = \int_\mathcal{D} q_n \, v_h \, dr - \sum_{\kappa\in\mathcal{M}_h} \left[\sum_{e\in\mathcal{E}_h\cap\mathcal{E}_h^-(\kappa)} \int_e (\vec{\Omega}_n \cdot \vec{n}) \, \phi_{n,h}^- \, v_h^+ \, ds \right]
\end{aligned} \tag{3}$$

Notice that this formulation is stable in a stronger norm than the $L^2(\mathcal{D})$-norm and therefore avoids possible nonphysical oscillations in the numerical solution [5]. This equation is solved elementwise according to a mesh sweeping strategy in such a way that the exterior traces $\phi_{n,h}^-$ on the inflow boundary of an element $\kappa \in \mathcal{M}_h$ are known when this element is calculated.

Remark : The Discontinuous Galerkin approximation of the discrete ordinate transport equation (3), showed in this paper, seems to be very similar to the variational formulation of the Arbitrarily High Order Transport method of the Nodal type (AHOT-N) [8, 9]. Even though the nodal method used in AHOT-N is quite different from a classical Discontinuous Galerkin method, the AHOT-N solution is equivalent to a non-stabilized Discontinuous Petrov Galerkin (DPG) projection, as shown in [8].

The qualitative mathematical difference between DPG methods and the more widely used Discontinuous Galerkin methods is that in Discontinuous Galerkin methods the test and the trial functions spaces are equal, while in DPG the weighting test functions are selected from a different class of functions that the approximate solution. The finite element test space chosen for AHOT-N is the space of discontinuous piecewise polynomials of degree p while the trial space is not polynomial and depends on each discrete ordinate $\vec{\Omega}_n$, *i.e.* the trial space is different for each direction of the unitary sphere.
In this paper, V_h^p, the space of discontinuous piecewise polynomials of degree p, define the trial functions as well as the test functions. This space is easier to compute and allow us to use a particular polynomial basis well adapted to hp-refinement, as we will see in the next section.

3. HIERARCHICAL POLYNOMIAL BASIS

In this section we describe succintly the polynomial basis used in our implementation of the Discontinuous Galerkin method and introduce the related notations. As we intend to have $p-$refinement capability, we choose hierarchical basis of the space of polynomials $Q_p(\hat{\kappa})$ on the reference element $\hat{\kappa}$, complete to the requested polynomial order p. These basis, denoted $\Xi_p(\hat{\kappa}) = \{f_i\}_{i\in[1,\dim\left(Q_p(\bar{\hat{\kappa}})\right)]}$, are constructed such that :

$$\Xi_p(\hat{\kappa}) \subset \Xi_{p+1}(\hat{\kappa}), \qquad \forall p \in \mathbb{N} \tag{4}$$

Following Shephard *et al.*[10], they are based on the topological hierarchy of mesh entities (vertices, edges and cells) which define the closure of an element. Taking into account the first-order adjacencies between these mesh entities, we can define the closure of each cell $\kappa \in \mathcal{M}_h$. For the sake of simplicity, we only deal here with the reference element $\hat{\kappa}$. The closure of this latter can then be specified as :

$$\bar{\hat{\kappa}} = \left\{M^2_{\hat{\kappa}}, \partial M^2_{\hat{\kappa}}\right\} = \left\{M^2_{\hat{\kappa}},\, M^2_{\hat{\kappa}}\{M^1_{\hat{\kappa},j'}\}, \ldots,\, M^2_{\hat{\kappa}}\{M^0_{\hat{\kappa},j'}\}\right\} \tag{5}$$

where $M^2_{\hat{\kappa}}\{M^{d'}_{\hat{\kappa},j'}\}$ is the $(j')^{\text{th}}$ entity of dimension d' bounding the reference element $\hat{\kappa}$.
Then, the polynomial basis of $Q_p(\hat{\kappa})$, $p \in \mathbb{N}$, are obtained by associating shape functions to these entities. Shape function construction must consider that topological entities in $\bar{\hat{\kappa}}$ can have independent polynomial order. Then, recalling (5), the i^{th} function associated to $M^{d'}_{\hat{\kappa},j'} \in \bar{\hat{\kappa}}$, denoted $f_i(M^{d'}_{\hat{\kappa},j'})$, is decomposed as :

$$f_i(M^{d'}_{\hat{\kappa},j'}) = \vartheta(M^{d'}_{\hat{\kappa},j'},\, M^2_{\hat{\kappa}})\, g_{i'}(M^{d'}_{\hat{\kappa}})$$

where :

- $\vartheta(M^{d'}_{\hat{\kappa},j'},\, M^2_{\hat{\kappa}})$ is a blending function defined on the reference element specific to $M^{d'}_{\hat{\kappa},j'}$ and independent of the polynomial order of $f_i(M^{d'}_{\hat{\kappa},j'})$;
- $g_{i'}(M^{d'}_{\hat{\kappa}})$ is the $(i')^{\text{th}}$ mesh entity level function dependent of the polynomial order of $f_i(M^{d'}_{\hat{\kappa},j'})$ and uniquely defined for all elements connected to $M^{d'}_{\hat{\kappa},j'}$.

Moreover, the blending functions $\vartheta(M^{d'}_{\hat{\kappa},j'},\, M^2_{\hat{\kappa}})$, $M^{d'}_{\hat{\kappa},j'} \in \bar{M}^2_{\hat{\kappa}}$, ensure that each shape function $f_i(M^{d'}_{\hat{\kappa},j'})$ vanishes over all lower order bounding entities except $M^{d'}_{\hat{\kappa},j'}$, *i.e.* :

$$f_i(\vec{r}) = 0 \qquad \forall \vec{r} \in \partial M^2_{\hat{\kappa}} \setminus M^{d'}_{\hat{\kappa},j'}$$

For example, the blending function defined on $\hat{\kappa}$ specific to itself is given by :

$$\vartheta(M^2_{\hat{\kappa}},\, M^2_{\hat{\kappa}}) = \frac{1}{4}(\xi_1^2 - 1)(\xi_2^2 - 1)$$

where $\xi_i \in [-1\,,1]$, $i = 1, 2$, are the local coordinates of the reference element.
This property is of particular interest in our case while propagating the flux from one cell to the other through the boundary trace.

The entity level functions can be comprised of any set of hierarchical basis functions, and are of order $p - q$ where q is the order of the blend. The entity level functions used here are based on standard Legendre polynomials. For example, the mesh entity level functions of order $k \geq 2$ associated to edges and to $\hat{\kappa}$ are given by :

$$\begin{aligned} g_0(M^1_{\hat{\kappa}}) &= Q_{k-2}(\hat{\xi}), \\ g_{i'}(M^2_{\hat{\kappa}}) &= Q_{k_1-2}(\xi_1)Q_{k_2-2}(\xi_2) \qquad \text{for } 2 \leq k_1, k_2 \leq k \end{aligned}$$

where $\hat{\xi} \in [-1\,,1]$ is the local coordinate associated to edges, $Q_{k-2}(\xi_i)$, $i = 1, 2$, is defined as :

$$\begin{aligned} \frac{\xi_i^2 - 1}{2} Q_{k-2}(\xi_i) &= \sqrt{\frac{2k-1}{2}} \int_{-1}^{\xi_i} P_{k-1}(t)dt, \qquad k \geq 2 \\ \text{or equivalently, } Q_{k-2}(\xi_i) &= \frac{\sqrt{2(2k-1)}}{k(k-1)} \frac{d}{d\xi_i} \left(P_{k-1}\right)(\xi_i), \qquad k \geq 2 \end{aligned}$$

and P_{k-1} is the Legendre polynomial of order $k - 1$.

The mapping from the reference element to another element $\kappa \in \mathcal{M}_h$ is the standard Q_1 mapping.

4. CELL INTERFACE TRANSFORMATION

Let us now suppose that $\mathcal{M}_h$ is non-conforming. Let Υ be the interface of two different subdomains of $\mathcal{M}_h$, $\mathcal{S}_1 = \bigcup_i \kappa_i$ and $\mathcal{S}_2 = \bigcup_j \kappa_j$, *i.e.* $\Upsilon = \mathcal{S}_1 \cap \mathcal{S}_2$. As $\mathcal{M}_h$ is non-conforming, Υ is partitionned in two different ways :

$$\mathcal{P}_1 = \{e : e \in \mathcal{E}_h(\mathcal{S}_1) \cap \Upsilon\} \quad \text{and} \quad \mathcal{P}_2 = \{e : e \in \mathcal{E}_h(\mathcal{S}_2) \cap \Upsilon\}$$

Thus, two different sets of shape functions are associated to $\mathcal{P}_1$ and $\mathcal{P}_2$ respectively :

$$\Xi_p(\mathcal{P}_1) = \{f_k\}_{k\in[1,N_p]} \quad \text{and} \quad \Xi_{p'}(\mathcal{P}_2) = \{g_{k'}\}_{k'\in[1,N_{p'}]}$$

where $N_p = \max_i (N_{p_i}) = \max_{i,\,\kappa_i\in\mathcal{S}_1} [\dim (Q_p(\kappa_i))]$ and $N_{p'} = \max_j \left(N_{p'_i}\right) = \max_{j\,\kappa_j\in\mathcal{S}_2} [\dim (Q_p(\kappa_j))]$.
Then, a mapping is required : the mapping transforming a linear combination $f(\vec{r})$ of shape functions $f_k(M^1_{\kappa_i})$, that we will denote for the sake of simplicity f^i_k, associated to $\Xi_p(\mathcal{P}_1)$

$$f(\vec{r}) = \sum_i^{N_i} \sum_k^{N_{p_i}} a^i_k f^i_k(\varsigma(\vec{r}))$$

into a linear combination $g(\vec{r})$ of shape functions $g_{k'}(M^1_{\kappa_j})$, that we will denote for the sake of simplicity $g^j_{k'} \in \Xi_{p'}(\mathcal{P}_2)$

$$g(\vec{r}) = \sum_{j}^{N_j} \sum_{k'}^{N_{p'_j}} b^j_{k'} g^j_{k'}(\varsigma(\vec{r})).$$

In the previous relations $N_i = \dim(\mathcal{P}_1)$ and $N_j = \dim(\mathcal{P}_2)$, ς stands for the mapping from the edge $e \in (\mathcal{P}_i)$, $i = 1, 2$, to the reference edge $\hat{e}$. The coefficients of $f(\vec{r})$ can be obtained from coefficients $b^j_{k'}$, $j = 1, \ldots, N_j$, $k' = 1, \ldots, N_{p'_j}$, in the following manner :

$$a^i_k = \sum_{j}^{N_j} \sum_{k'}^{N_{p'_j}} b^j_{k'} T^{j,i}_{k',k}, \qquad i = 1, \ldots, N_i,\ k = 1, \ldots, N_{p_i}$$

where the coupling coefficients $T^{j,i}_{k',k}$ are calculated minimizing in L^2-norm the difference between $f(\vec{r})$ and $g(\vec{r})$ [11].

Continuous finite elements require that the local shape functions of subdomains $\mathcal{S}_1$ and $\mathcal{S}_2$ be locally modified to taking into account the mesh refinement. The great advantage of Discontinuous Galerkin finite element method is that each cell is treated separately thanks to the concept of interior and exterior traces. Thus, the shape functions associated to the subdomains $\mathcal{S}_1$ and $\mathcal{S}_2$ does not have to be modified. Moreover, this mapping is well adapted to hierarchical basis as the shape functions are defined for all mesh entities, and in particular for each $e \in \mathcal{P}_1$ and $e \in \mathcal{P}_2$. The spatial discretization used in this paper allows an easy implementation when transforming $f(\vec{r})$ in $g(\vec{r})$.

5. NUMERICAL RESULTS

The numerical scheme presented in this paper has been implemented in the ERANOS code system [12, 13] dedicated to fast reactor analysis and validated on a set of one-speed benchmark with the comparison to a classical S_N method using the Diamond Differencing scheme as spatial approximation.
We present in this section some numerical results which show the good convergence properties of this scheme and the purpose of using h- and p-refinement.

5.1. One-group eigenvalue benchmark

The one-group eigenvalue benchmark we used was proposed in [14]. Its geometry and cross-sections are given in Fig. 1 and Table I respectively. It is surrounded by void boundary conditions and has a regular cell pitch of 40 cm. An S_8 approximation is chosen with an angular discretization based on a level-symmetric quadrature.

The numerical scheme presented here is first validated comparing the numerical results obtained with this latter and those obtained with the Diamond Differencing scheme as spatial approximation.
Then, in order to highlight the h- and p-convergence properties of the Discontinuous Galerkin spatial scheme, we use different conforming and non-conforming meshes and different

Table I. Macroscopic P_1 cross-sections (in cm^{-1})

material	Σ_t	Σ_s^0	Σ_s^1	$\nu\Sigma_f$
mix 3	0.075	0.0	0.0	0.0
mix 2	0.025	0.024	0.006	0.0
mix 1	0.025	0.013	0.0	0.0155

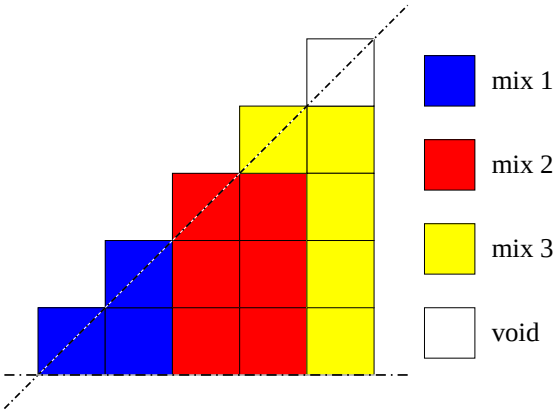

Figure 1. One-group eigenvalue benchmark geometry

polynomial orders. Meshes are obtained by subdividing in $n \times n$ each cell of the 5×5 cartesian geometry.

The convergence is presented in terms of the maximum $\epsilon_{\max}$, the average $\bar{\epsilon}$ and the discrete L^2 norm errors on the absorption rate τ_κ over the geometry cells i.e.

$$\epsilon_{\max} = \max_{\kappa \in \mathcal{M}_h} \left(|\epsilon_\kappa| \right), \tag{6}$$

$$\bar{\epsilon} = \frac{1}{|\mathcal{D}|} \sum_{\kappa \in \mathcal{M}_h} |\kappa| |\epsilon_\kappa|, \tag{7}$$

$$||\epsilon||_{L^2} = \sqrt{\sum_{\kappa \in \mathcal{M}_h} |\kappa| \epsilon_\kappa^2}, \tag{8}$$

where $\epsilon_\kappa = \dfrac{\tau_\kappa - \tau_\kappa^{\text{ref.}}}{\tau_\kappa^{\text{ref.}}}$ and $|\kappa|$ is the volume of the geometry cell κ while $|\mathcal{D}| = \displaystyle\sum_{\kappa \in \mathcal{M}_h} |\kappa|$ is the geometry total volume.

The results are presented in Table II; DD denotes the Diamond Differencing scheme while DG-p refers to the Discontinuous Galerkin scheme of order p. The discrete L^2 norms of the absorption rate as function of the polynomial order p and the number of cells are depicted in Fig. 2 and Fig. 3

respectively. The reference is taken as the Discontinuous Galerkin scheme of order 6 on the 8×8-discretized mesh. Both the h- and p-convergence can be observed and the interest of both h- and p-refinement is highlighted. Indeed, as the maximum error is located in mixture 3, increasing locally the polynomial order (see red values in Table II) or refining locally the spatial mesh (see blue values in Table II) allows to obtain the same accuracy on the error than refining each cell of the mesh or increasing the polynomial order everywhere.

Table II. hp-convergence on the absorption rate

n	$\epsilon_{\max}$ (%) / $\bar{\epsilon}$					
	DD	DG-1	DG-$1/2^a$	DG-2	DG-$2/4^a$	DG-4
1	157.9/28.04	16.61/3.71	7.18/1.32	6.18/1.01	1.14/0.13	1.13/0.12
1 / 2^b		1.52/0.58	1.28/0.57	0.25/0.05	0.13/0.03	
2	21.33/2.96	0.42/0.15	0.35/0.07	0.24/0.03	0.01/0.002	$0.002/4{\cdot}10^{-4}$
3	6.23/1.31	0.22/0.08		0.01/0.002	$0.003/9{\cdot}10^{-4}$	
2 / 4^b		0.25/0.07	0.20/0.06	0.09/0.002	0.01 / 0.002	
4	0.42/0.91	0.08/0.03	0.03/0.009	$0.004/8{\cdot}10^{-4}$		
6	0.50/0.20	0.03/0.01	0.009/0.003	$7{\cdot}10^{-4}/1{\cdot}10^{-4}$		
8	0.19/0.10	0.01/0.005				

[a] DG-p/q indicates order p (resp. order q) in mixtures 1 and 2 / (resp. mixture 3).

[b] n/m indicates a $n \times n$-split (resp. $m \times m$-split) in mixtures 1 and 2 (resp. mixture3).

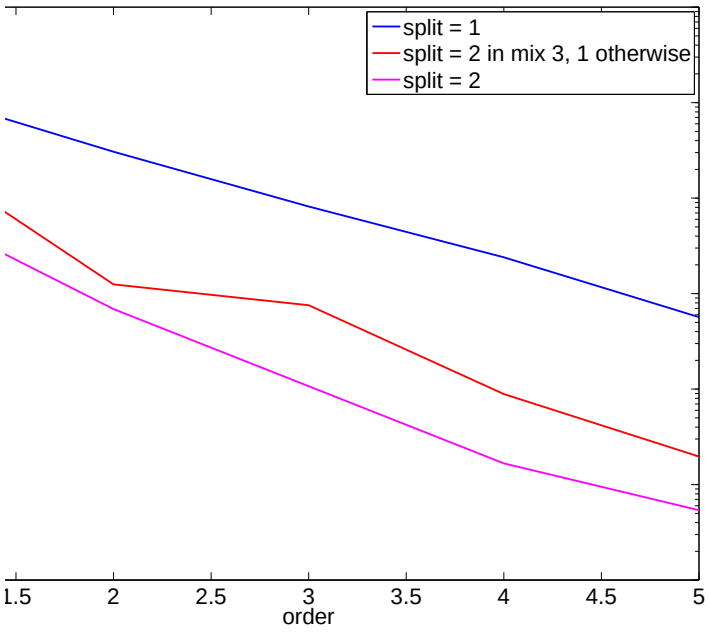

Figure 2. L^2 error norm of the absorbtion rate as a function of p

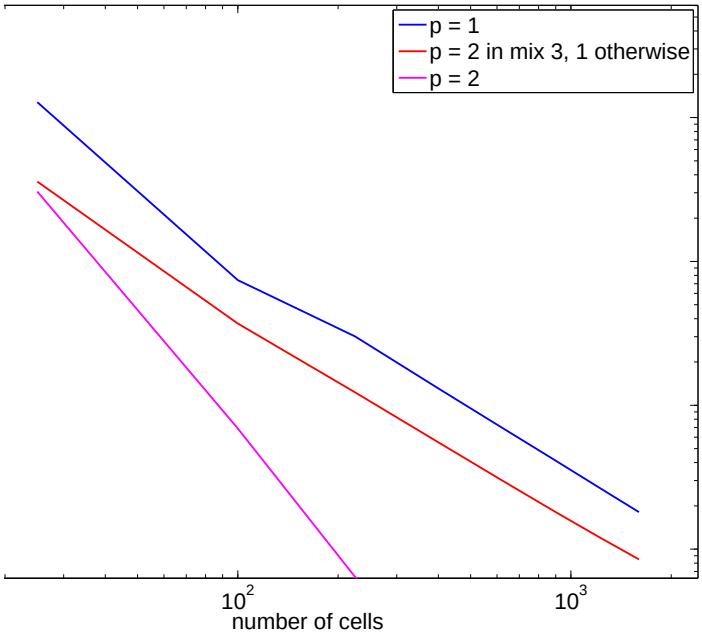

Figure 3. L^2 error norm of the absorbtion rate as a function of number of cells

5.2. One group shielding benchmark

The shielding benchmark we used is proposed in [9]. It consists of an inner square with side length of $10\,\text{cm}$ with total cross section $\Sigma_t = 1\,\text{cm}^{-1}$ and scattering cross section $\Sigma_s^0 = 0.5\,\text{cm}^{-1}$ with an isotropic source $Q_n = 4\,\pi\,\text{cm}^{-3}\cdot\,\text{s}^{-1}$, surrounded by an absorber with total cross section $\Sigma_t = 2\,\text{cm}^{-1}$ and scattering cross section $\Sigma_s^0 = 0.025\,\text{cm}^{-1}$. The external dimensions of the absorber are $20\,\text{cm} \times 20\,\text{cm}$, with vacuum external boundary conditions. An S_4 approximation is chosen with an angular discretization based on a level-symmetric quadrature.
The reference solution was generated on a uniform mesh of 200×200 cells with the Discontinuous Galerkin scheme of order 6. The numerical solutions were computed over one fourth of the domain using reflective boundary conditions. The reference solution is shown on Fig. 4.

The goal of this benchmark is to highlight the purpose of the hp-refinement, *i.e.* show that applying an hp-refinement *ad hoc* we can both get a better approximation of the reference solution and a lower computational cost, than without these numerical techniques. The results are presented in terms of the discrete L^2 error norm on the cell averaged flux and of the cell wise error.
Let $\bar{\phi}_{ref}$ and $\bar{\phi}_h$ denote the cell averaged reference and numerical solutions, respectively, the

discrete L^2 error norm on the cell averaged flux and the cell wise error are given by :

$$||\epsilon||_{L^2}^2 = \sum_{\kappa \in \mathcal{M}_h} \sum_{m=1}^{N(N+2)/2} w_m \left(|\bar{\phi}_{ref} - \bar{\phi}_h|\right)^2 |\kappa|, \tag{9}$$

$$\epsilon_\kappa = \sum_{m=1}^{N(N+2)/2} w_m |\bar{\phi}_{ref} - \bar{\phi}_h|, \qquad \forall \kappa \in \mathcal{M}_h \tag{10}$$

where w_m, $m = 1, \ldots, N(N+2)/2$ are the weights of the level symmetric quadrature and $|\kappa|$ is the volume of the cell $\kappa \in \mathcal{M}_h$.

At the top of Fig. 5.2, we present the cell wise error obtained with a uniform mesh of 40×40 cells and a Discontinuous Galerkin scheme of order 4 (40400 dofs). The discrete L^2 error norm on the cell averaged flux is $||\epsilon||_{L^2} = 3.59 \cdot 10^{-3}$. The error is localised in the corner of the source region where steepest gradients are present and at the top right corner of the domain, *i.e.* the furthest point from the source.
At the bottom of Fig. 5.2, we present the cell wise error obtained with a non-conforming mesh. In order to deal with the steep gradients at the boundaries of the source, we refine the spatial mesh close to the source and use a lower order of polynomials ($p = 2$). Elsewhere, the mesh is coarser and the order of the numerical scheme is higher ($p = 4$). The discrete L^2 error norm on the cell averaged flux, $||\epsilon||_{L^2} = 3.07 \cdot 10^{-3}$, and the cell wise error at the corner of the source are lower than in the uniform case. Using hp-refinement in this way, we obtain with less degrees of freedom (36272 dofs), *i.e.* with a lower computational cost, a better estimate of the solution of the problem, in spite of a slightly higher local error at the boundaries of the source. This problem is probably due to a worse approximation of the flux close to these regions in the coarser mesh.

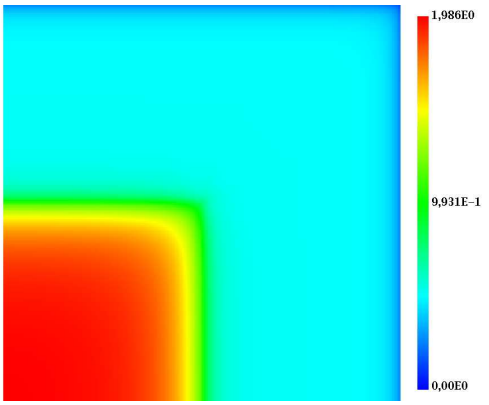

Figure 4. Reference solution of the one group shielding benchmark

Remark : We talk here about the computational cost of this numerical scheme without giving a number of operations or an executation time. In fact, actually, the implementation of this numerical scheme is not optimized, so the executation time or the number of operations would not be meaningful.

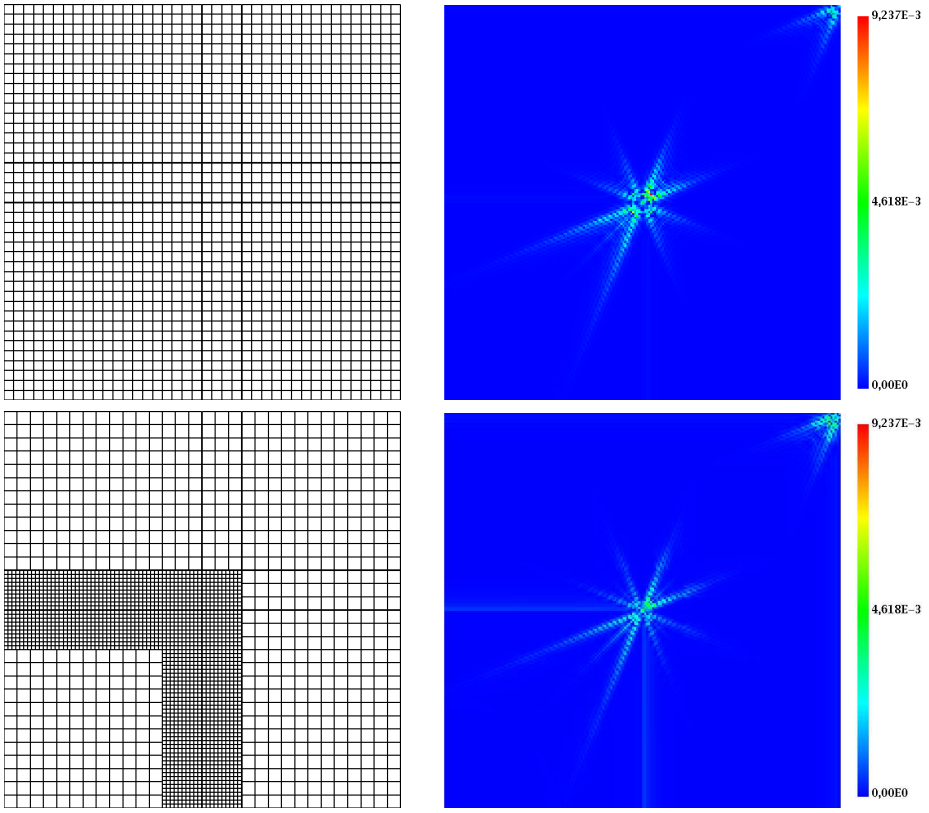

Figure 5. Conforming and non-conforming meshes and relative cell wise errors

6. CONCLUSIONS

In this paper, we have presented a numerical scheme intended for the modeling of core geometries based on homogeneous Cartesian assemblies. The discrete ordinate method is used as angular approximation and the spatial discretization is based on discontinuous finite elements. In order to have p-refinement capability, we have chosen a hierarchical polynomial basis based on Legendre polynomials. The h-refinement capability is also available and an L^2-norm minimization technique is used to treat easily non conforming meshes.
This method is easily extendible to three-dimensional case. Indeed, the discontinuous finite element discretization presented here is strictly the same in both two-dimensional and three-dimensional cases, as for hierarchical polynomial basis, we only need to introduce faces to the topological hierarchy of mesh entities.
This numerical scheme has been sucessfully implemented in the ERANOS code system and validated on several benchmarks. This validation confirms the good convergence properties of the method and highlight the purpose of hp-refinement.
It has been naturally extended to a three-dimensional hexahedral grid simply by implementing the hierarchical polynomial basis on the hexahedron reference element.
The application of hp-adaptive mesh refinement strategies to this numerical scheme is still under study.

REFERENCES

[1] A. Hébert, *"Applied Reactor Physics"*, Report IGE-281(Rev.2), Institut de Génie Nucléaire, Ecole Polytechnique de Montréal (2006).

[2] Y. Wang, J. Ragusa, M. DeHart, "Xuthos: A Discontinuous Galerkin Transport Solver for NEWT Based On Unstructured Triangular Meshes", *Proceedings of International Conference on the Physics of Reactors "Nuclear Power: A Sustainable Resource"*, Switzerland, September 14-19 (2008).

[3] C. Aussourd, "Styx: A multidimensional AMR S_N Scheme", *Nucl. Sc. Eng.*, **143**, pp. 281-290 (2003).

[4] I. Zmijarevic, "IDT solution to the 3D transport benchmark over a range in parameter space", *Proceedings of International Conference on the Physics of Reactors "Nuclear Power: A Sustainable Resource"*, Switzerland, September 14-19 (2008).

[5] F. Brezzi, L.D. Marini, E. Süli, "Discontinuous Galerkin methods for first-order hyperbolic problems", *Math. Models Methods Appl. Sci.*, **14**, pp. 1893-1903 (2004).

[6] B. Cockburn, C.W. Shu, "The local discontinuous Galerkin method for time-dependent convection-diffusion systems", *SIAM J. Numer. Anal.*, **35**, pp. 2240-2463 (1998).

[7] B.Q. Li, *"Discontinuous Finite Elements in Fluid Dynamics and Heat Transfer"*, Computational Fluid and Solid mechanics, Springer, (2006).

[8] J.I. Duo, *"Error estimates for Nodal and Short Characteristics Spatial Approximations of 2-D Discrete Ordinates Method"*, Dissertation, The Pennsylvania State University (2008).

[9] J.I. Duo, Y.Y. Azmy, L.T. Zikatanov, "A posteriori error estimator and AMR for discrete ordinates nodal transport methods", *Proceedings of International Conference on the Physics of Reactors "Nuclear Power: A Sustainable Resource"*, Switzerland, September 14-19, Vol.2 (2008).

[10] M.S. Shephard, S. Dey, J.E. Flaherty, "A straightforward structure to construct shape functions for variable p-order meshes", *Comput. Methods Appl. Mech. Engrg.*, **147**, pp. 209-233 (1997).

[11] E. Girardi, *"Couplage de méthodes et décomposition de domaine pour la résolution de l'équation du transport des neutrons"*, PhD thesis, Université d'Evry Val d'Essonne (2004).

[12] G. Rimpault, D. Plisson, J. Tommasi, J.M. Rieunier and R. Jacqmin, "The ERANOS code and data system for fast reactor analyses", *Proceedings of International Conference on the New Frontiers of Nuclear Technology*, Korea, October 7-10 (2002).

[13] J.M. Ruggieri, J. Tommasi, J.F. Lebrat, C. Suteau, D. Plisson-Rieunier and C. De Saint Jean, "ERANOS-2.1: The international code system for GEN-IV fast reactor analysis", *Proceedings of International Congress on Advances in Nuclear Power Plants*, USA, June 4-8 (2006).

[14] A. Hébert, "The Search for Superconvergence in Spherical Harmonics Approximations", *Nucl. Sc. Eng.*, **154**, pp. 134-173 (2006).